The International Journal of Advanced Manufacturing Technology
https://doi.org/10.1007/s00170-022-10652-y

ORIGINAL ARTICLE

Optimization and characterization of T-joint laser welds for aluminum fin heat sink with copper base

Chin-Lung Chang[1] · Yi-Hong Cheng[1,2] · Hsuan-Kai Lin[2]

Received: 15 October 2022 / Accepted: 2 December 2022

Abstract

Heat sink assemblies consisting of an A6061-T6 aluminum alloy fin and a C1100 copper base are prepared by T-joint welding using a near continuous-wave fiber laser system. The effects of the welding parameters on the tensile strength and heating rate of the heat sink assembly are investigated and compared. It is shown that the maximum tensile strength and heating rate are obtained using a laser power of 220 W, a pulse width of 8 ms, a welding speed of 2 mm/s, and an incident angle of 60°. The thermal conductivity of the heat sink prepared using the optimal welding parameters is shown to be in good agreement with the ANSYS Fluent simulation results obtained under the assumption of an ideal, defect-free joint between the copper base and aluminum fin. The tensile strength and heating rate using the optimal welding parameters are 24.31 MPa and 41.2 °C/10^2 S, respectively. The optical microscopy (OM) images show that the thickness of the intermetallic compound (IMC) layer formed at the interface between the aluminum fin and the copper base varies with the welding parameters and has a value of approximately 6 μm under the optimal welding conditions. The energy dispersive spectrometry (EDS) results and X-ray diffraction (XRD) analysis results reveal that the welding bead consists mainly of Cu, Al, and Al_2Cu phases.

Keywords Fiber laser · Dissimilar metal welding · Intermetallic compound · Cooling fin · T-joint laser welding

1 Introduction

Laser technologies, characterized by high energy density, good repeatability, a rapid processing time, and high precision, are used for many applications nowadays, including cutting, welding, surface treatment, and photo-etching. Traditional welding processes, such as tungsten inert gas (TIG) welding or spot welding, produce a large heat-affected zone (HAZ) and therefore prompt an uneven microstructure and non-uniform properties in the vicinity of the weld. Thus, for many applications, particularly those requiring high-precision welds, laser beam welding (LBW) is commonly preferred. Compared to traditional welding techniques, LBW has a lower heat input, a narrower HAZ, and a thinner intermetallic compound (IMC) layer. Hence, LBW has received extensive attention in the literature in recent decades [1–4]

The persistent trend toward device miniaturization and increased functionality and power has led to the need for advanced thermal management solutions in the electronics and semiconductor industries. Finned heat sinks continue to be one of the most common methods for meeting this need. Various studies have shown that the heat dissipation performance of finned heat sinks can be improved by perforating the fins in the longitudinal direction or offsetting the alternate fins within the fin array [5, 6]. Other researchers have shown that the heat transfer performance can be enhanced by mounting an aluminum fin with a high dissipation capacity on a copper base with a high thermal conductivity [7, 8]. However, copper has high surface reflectivity, while aluminum and copper have poor miscibility. Thus, forming dissimilar welds of copper and aluminum using the laser welding technique is challenging [9–11], and the formation of IMCs frequently degrades the welding quality [12–15]. Choudhury [16] investigated the mechanical properties of friction stir-welded Al–Cu lap joints. The results showed that the maximum hardness of the welded joints occurred in the interface region due to

✉ Hsuan-Kai Lin
HKLin@mail.npust.edu.tw

[1] Department of Vehicle Engineering, National Pingtung University of Science and Technology, Pingtung 912, Taiwan

[2] Graduate Institute of Materials Engineering, National Pingtung University of Science and Technology, Pingtung 912, Taiwan

Published online: 12 December 2022

the formation of IMCs. For lower values of the welding speed, the formation of an IMC layer resulted in a low failure stress. Under higher welding speeds, micro-voids were formed, which similarly reduced the failure stress. Yan [17] used a laser micro-welding technique to form Al–Cu dissimilar joints. It was shown that the tensile strength of the joints was comparable to that of the Al base metal given an IMC layer thickness of 0.2 to 0.5 μm.

The problem of optimizing the LBW processing conditions for the dissimilar welding of copper and aluminum has attracted significant attention in the literature. Generally speaking, the laser focal position of the laser spot controls the aspect ratio of the melt pool [18, 19], while the laser power, pulse width, and welding speed [20, 21] collectively determine the susceptibility of the weld area to cracking [22, 23]. Moreover, the angle of incidence of the laser beam on the specimen surface has a direct

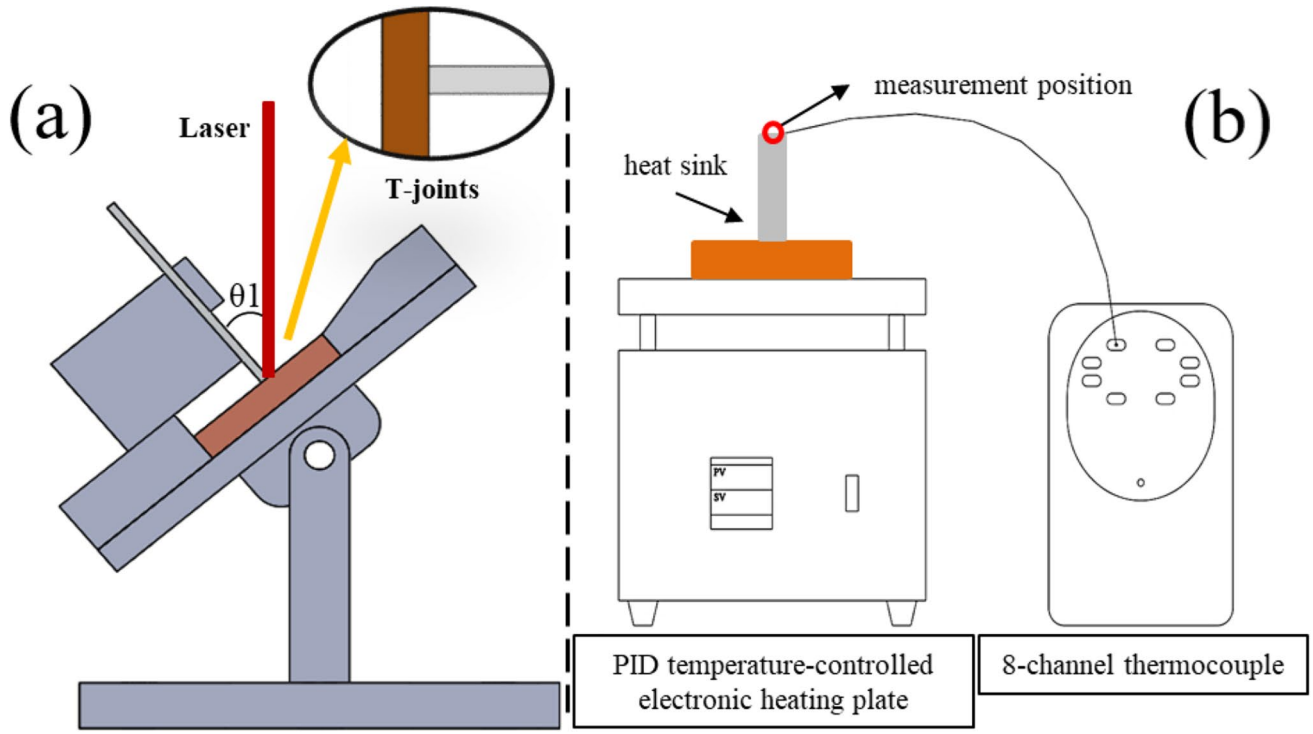

Fig. 1 Schematic illustrations of: (**a**) T-joint laser welding fixture, and (**b**) thermal conductivity test setup

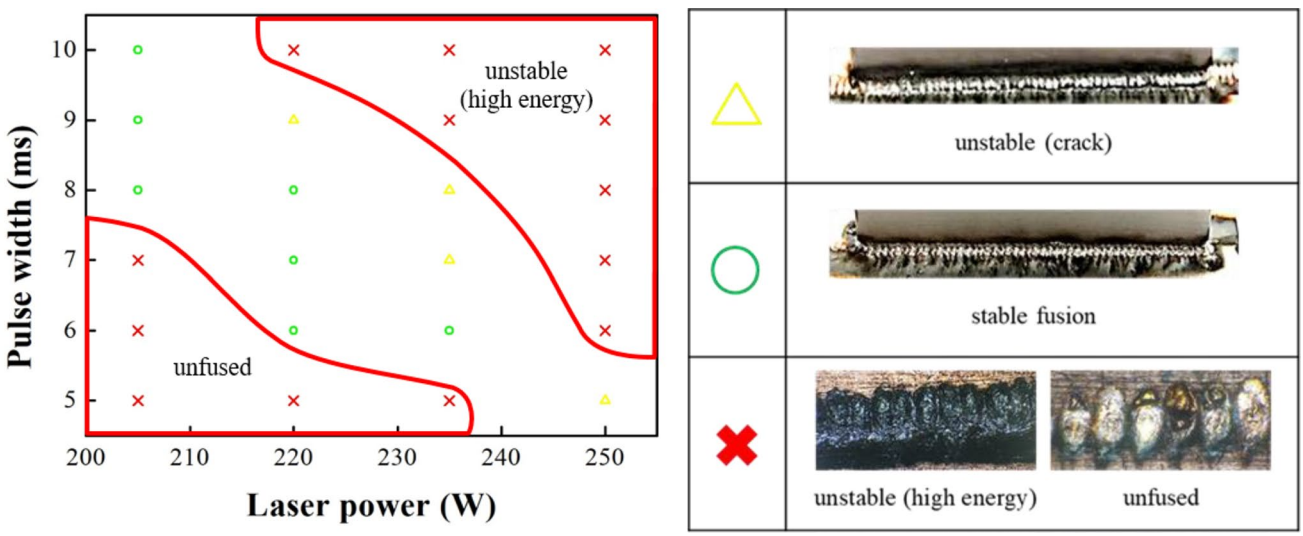

Fig. 2 Effects of laser power and pulse width on welding quality (unfused area, stable area, and unstable area)

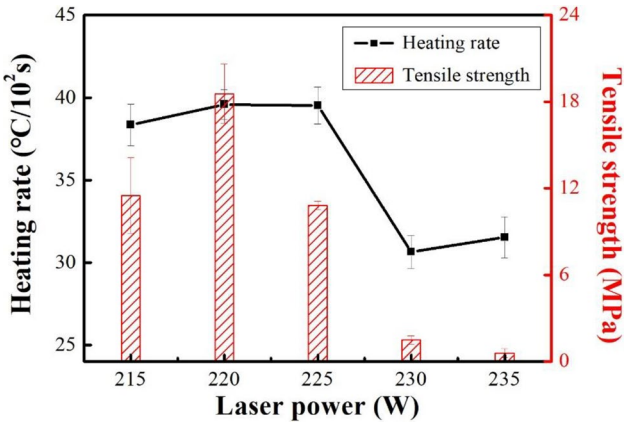

Fig. 3 Effects of laser power on heating rate and tensile strength of welded samples

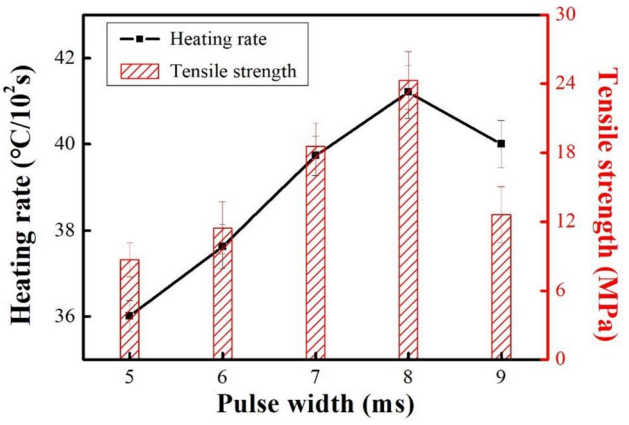

Fig. 5 Effects of laser pulse width on heating rate and tensile strength of welded samples

effect on the quality of the weld bead, and hence on the tensile properties of the joint [24]. The authors in [25–30] showed that a careful setting of the LBW parameters is thus essential in optimizing the energy density during the welding process and improving the quality of the weld as a result.

The hydrogen and magnesium vapor generated during the solidification process of aluminum alloys results in the formation of pores during the welding process. Moreover, a rapid solidification rate may result in crack initiation [31–33]. Hence, it is necessary to adjust the pulse width or laser preheating effect in such a way as to extend the solidification time and suppress the formation of defects [34]. The authors in [35] showed that the welding quality of dissimilar copper and aluminum joints can be improved by overlapping the two materials during the welding process in order to minimize the reflectivity effect. Consequently, the copper and aluminum dissimilar joints fabricated in industry nowadays are usually produced using a T-joint laser welding process [36].

The present study fabricates heat sinks consisting of a copper base and an aluminum fin using a near continuous-wave laser system and a T-joint arrangement of the base metals. The tensile strength and heating rate of the heat sinks are evaluated for various values of the laser power, pulse width, weld speed, and incident angle. The thermal conductivity of the heat sink fabricated using the optimal LBW parameters is compared with the ideal thermal conductivity predicted by ANSYS Fluent simulations. Moreover, the hardness profiles of the weld bead at different depths are evaluated by micro-Vickers hardness tests. Finally, the formation and composition of the IMC layer in the weld bead are examined by optical microscopy, energy dispersive spectrometry (EDS), and X-ray diffraction (XRD).

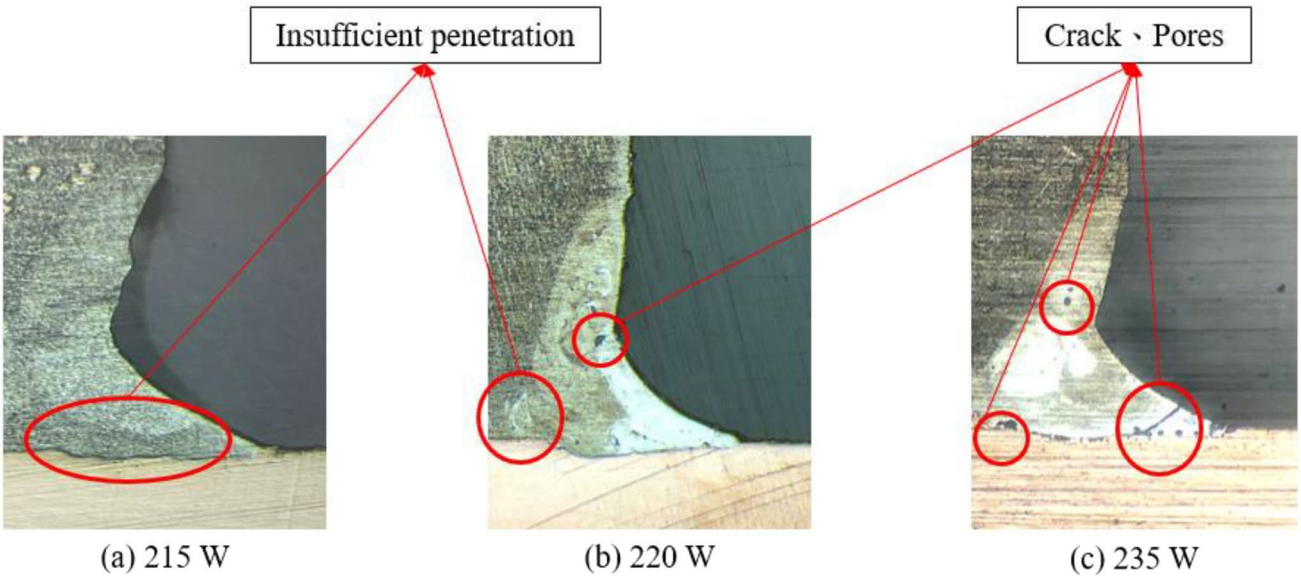

Fig. 4 Microstructures of weld beads produced with different laser powers: (**a**) 215 W, (**b**) 220 W, and (**c**) 235 W

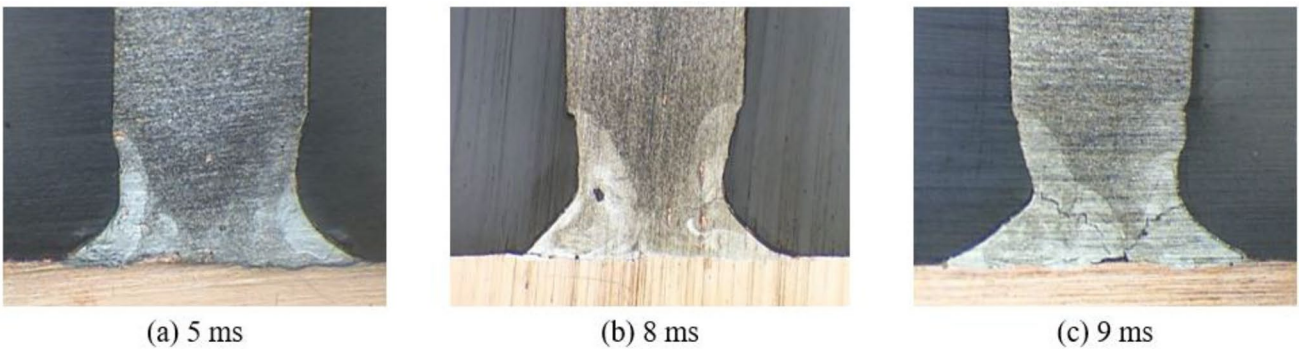

Fig. 6 Microstructures of weld beads produced with different pulse widths: (**a**) 5 ms, (**b**) 8 ms, and (**c**) 9 ms

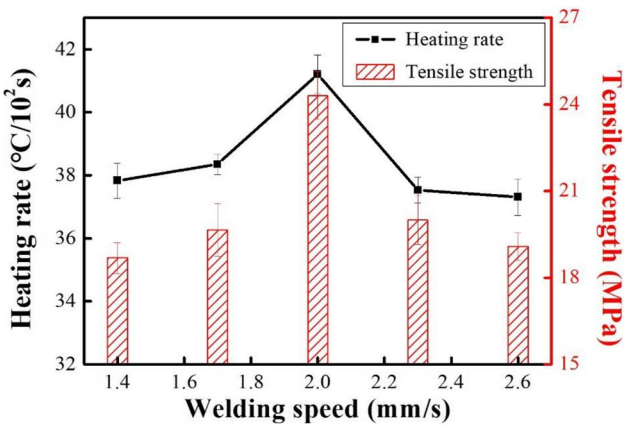

Fig. 7 Effects of welding speed on heating rate and tensile strength of welded samples

2 Experimental materials and procedures

The heat sinks comprised a 6061-T6 aluminum fin with dimensions of $40 \times 20 \times 1$ mm^3 welded to a C1100 copper base with a size of $40 \times 25 \times 5$ mm^3. Both materials were purchased from Yung Hsu Machinery Co., Ltd. (Taiwan) and were polished sequentially with 400# and 800# sandpapers and then cleaned with acetone prior to welding. As shown in Fig. 1a, the fin was mounted on the copper base using a T-type welding process. The welding procedure was performed using a near continuous-wave laser system (IPG Photonics, YLM-450/4500-QCW, US) with a wavelength of 1070 nm and a spot size of 0.5 mm. To investigate the effects of the LBW process parameters on the welding quality, welding trials were performed using laser powers of 215, 220, 225, and 235 W; pulse widths of 5, 6, 7, 8, and 9 ms; welding speeds of 1.4, 1.7, 2.0, 2.3, and 2.6 mm/s; and incident angles of 50, 55, 60, and 70°.

The tensile strengths of the various welded samples were evaluated using a self-made fixture. In addition, the heating rates were measured using the setup shown in Fig. 1b. Briefly, the PID temperature-controlled electronic heating plate was maintained at a constant temperature of 80 °C, and the thermocouple wire of an 8-channel thermocouple data logger was attached to the top of the aluminum fin. The heat sink was then placed on the heating plate, and the temperature at the top of the fin was measured continuously over a period of 3 min.

The hardness profile of the weld bead in the sample fabricated using the optimal processing parameters was examined using an HM-113 Vickers hardness tester under

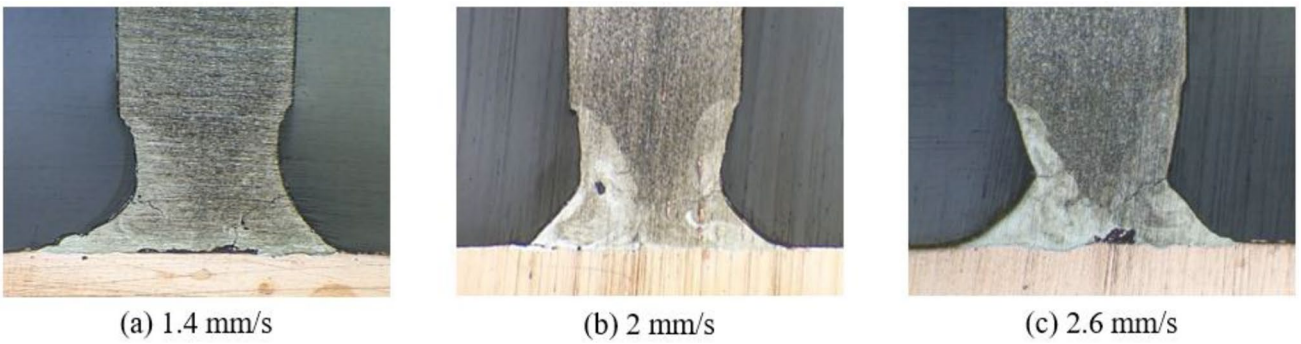

Fig. 8 Microstructures of weld beads produced with different welding speeds: (**a**) 1.4 mm/s, (**b**) 2 mm/s, and (**c**) 2.6 mm/s

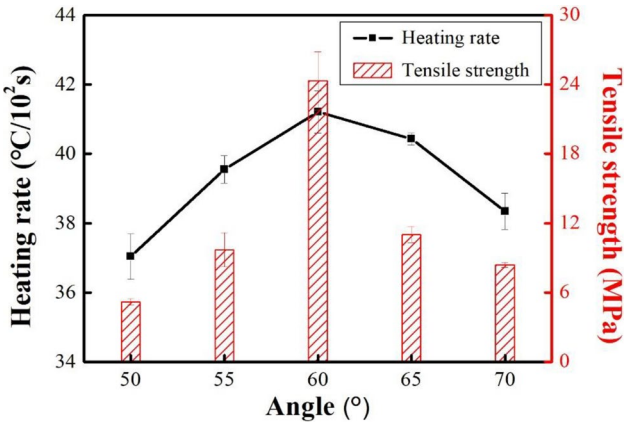

Fig. 9 Effects of laser incident angle on tensile strength and heating rate of welded samples

an indentation load of 0.05 kg and a loading time of 10 s. The weld bead sections in the various samples were polished and etched with Keller solution (1.5 ml hydrochloric acid, 1.0 ml 40% hydrofluoric acid, and 95 ml H_2O) for 1 s to reveal the Cu–Al IMC layer. The thickness of the IMC layer in each sample was measured under an optical microscope (OM, HRM-300, Huvitz). Finally, the composition of the IMC in the weld bead produced under the optimal conditions was determined by a JSM-7600F field emission scanning electron microscope (SEM) integrated with an energy dispersive spectrometer (EDS) and an X-ray diffractometer (Bruker, D8 Advance, Germany).

3 Results and discussion

Figure 2 shows the effects of the laser power and pulse width on the quality of the welding outcome (i.e., unfused, stable, and unstable). Note that the incident angle of the laser beam was 60° in every case, while the welding speed was 2 mm/s. The results indicate that, as the laser power increases, the pulse width should be reduced in order to avoid the formation of cracks in the weld bead. Moreover, low energy density welding conditions (i.e., a lower laser power and lower pulse width) should be avoided to prevent the formation of unfused welds.

Figure 3 shows the tensile strengths and heating rates of the samples processed using different laser powers in the range of 215–235 W. Note that pulse width and laser speed were 7 ms and 2 mm/s, respectively. As shown, the maximum tensile strength and heating rate are achieved for a laser power of 220 W. As the laser power increases to 225 W, the tensile strength and heating rate reduce only very slightly. However, as the laser power further increases to 235 W, both properties drop significantly. As shown in Fig. 4, for a lower laser power of 215 W, the weld bead has only poor penetration, and hence the tensile strength and heating rate are reduced. For a laser power of 220 W, the region of insufficient penetration is reduced, and the weld bead contains only a small number of defects. As a result, the mechanical and thermal properties are both improved. However, under the maximum laser power of 235 W, the weld bead contains a large number of pores and cracks, and thus both the tensile strength and the heating rate are seriously impaired.

Figure 5 shows the effect of the laser pulse width on the tensile strength and heating rate of the welded sample given a laser power of 220 W and a speed of 2 mm/s. As shown,

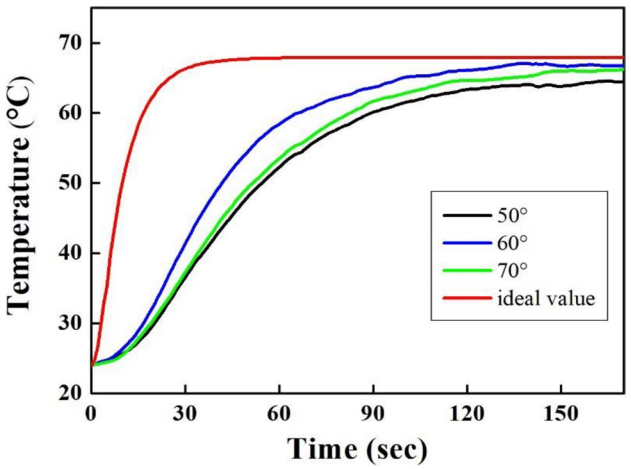

Fig. 11 Comparison of simulated ideal thermal conductivity curve and experimental curves for welded samples produced with different incident angles

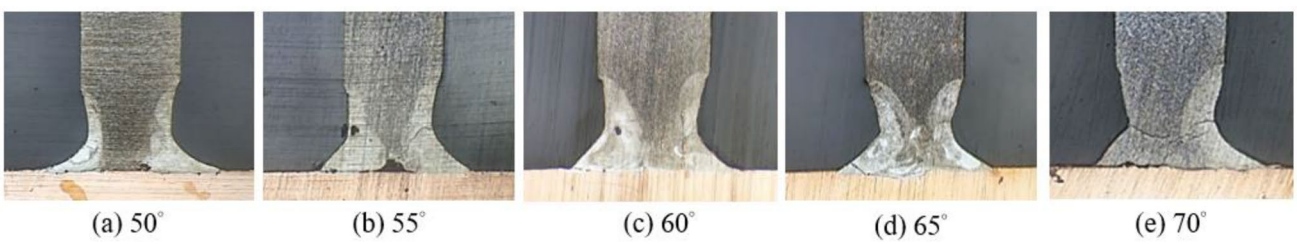

Fig. 10 Microstructures of weld beads produced with different incident angles: (**a**) 50°, (**b**) 55°, (**c**) 60°, (**d**) 65°, and (**e**) 70°

the maximum tensile strength and heating rate are obtained for a pulse width of 8 ms. In general, a longer pulse width increases the energy input to the weld bead and delays the solidification time of the molten pool. As a result, the generation of pores and cracks decreases [29, 30]. For a short pulse width of 5 ms, the weld bead contains almost no defects, as shown in Fig. 6a. However, the weld bead has poor penetration, and hence the tensile strength and heating

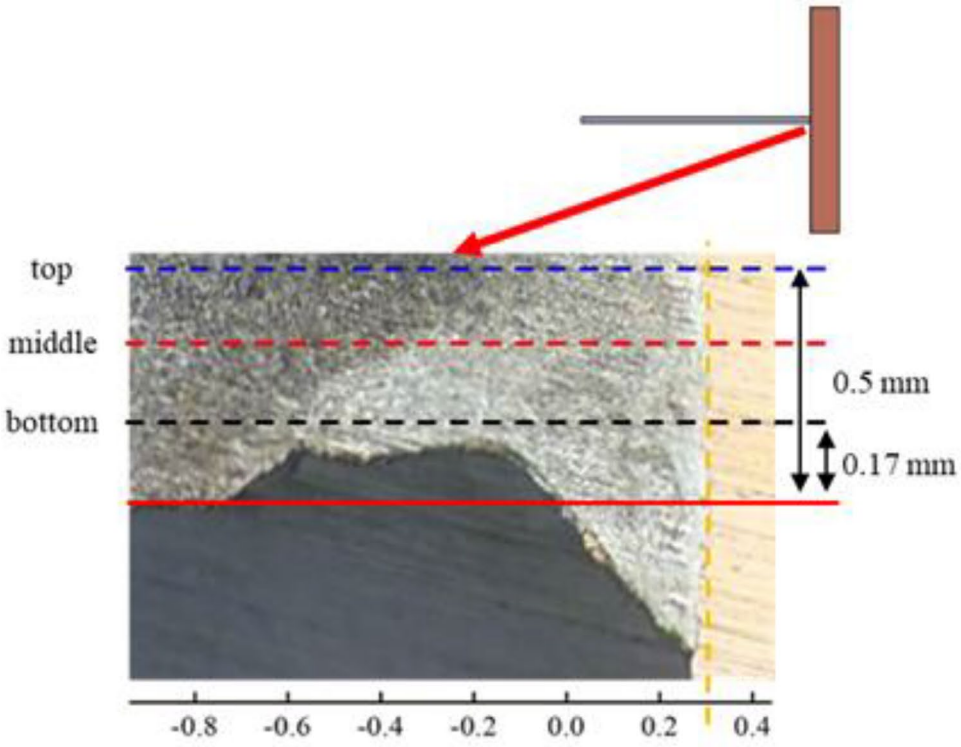

(a)

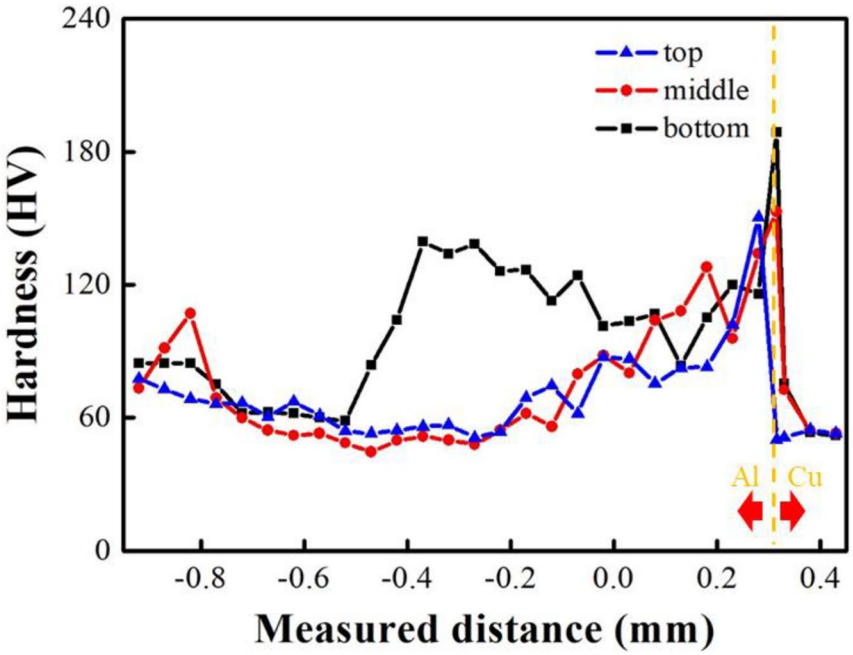

(b)

Fig. 12 (**a**) OM image of weld bead profile and (**b**) hardness profiles along various depth planes in (**a**)

rate are both reduced. The OM image in Fig. 6b confirms that a pulse width of 8 ms yields a good welding quality. However, for a high pulse width of 9 ms, the energy input is excessive, and thus severe cracking and a non-symmetric bead profile are produced, as shown in Fig. 6c.

Figure 7 shows the tensile strengths and heating rates of the samples produced using welding speeds of 1.4 to 2.6 mm/s, a laser power of 220 W, and a pulse width of 8 ms. It is seen that a welding speed of 2 mm/s results in the maximum tensile strength and heating rate. The OM image presented in Fig. 8b confirms that a welding speed of 2 mm/s results in a high quality weld. However, for a lower welding speed, the weld bead is incomplete (Fig. 8a), while for a high welding speed, the number of pores increases, as shown in Fig. 8c.

Finally, Fig. 9 shows the variation of the tensile strength and heating rate with the incident angle of the laser beam. The processing parameters are set as given a laser power of 220 W, a pulse width of 8 ms, and a speed of 2 mm/s. Note that the laser power, pulse width, and laser speed were set as 220 W, 8 ms, and 2 mm/s, respectively. It is seen that the maximum tensile strength and heating rate are obtained for an incident angle of 60° and have values of 24.31 MPa and 41.2 °C/10^2 S, respectively. Figure 10 presents the OM images of the corresponding weld beads. In general, the results show that a lower incident angle results in an incomplete welding of the joint (as shown in Fig. 10a, b), while a larger incident angle leads to cracking at the welding interface (see Fig. 10d, e).

Overall, the results presented in Figs. 2–10 show that the optimal parameter settings for the composite Cu–Al heat sink are a laser power of 220 W, a pulse width of 8 ms, a welding speed of 2 mm/s, and an incident angle of 60°. The ideal thermal conductivity of the composite heat sink was calculated by means of ANSYS Fluent simulations under the assumptions of a heat plate temperature of 80 °C, an ambient temperature of 24 °C, a natural convection cooling rate of 25 W/m^{2}K, and a perfect, defect-free joint between the copper base and aluminum fin. The simulation results showed that the top of the aluminum fin approached a steady-state temperature of approximately 68 °C (red line in Fig. 11). The thermal conductivities of the heat sink assemblies fabricated using the optimal focal position, laser power, pulse width, and welding speed were measured using the experimental setup shown in Fig. 1b for laser incident angles of 50°, 60°, and 70°, respectively. As shown by the blue line in Fig. 11, the measured thermal conductivity of the heat sink assembly fabricated using the optimal processing conditions (including an incident angle of 60°) approached the ideal value. Thus, the validity of the optimal processing conditions was confirmed.

Figure 12a presents an OM image of the weld bead profile in the sample prepared using the optimal parameter settings.

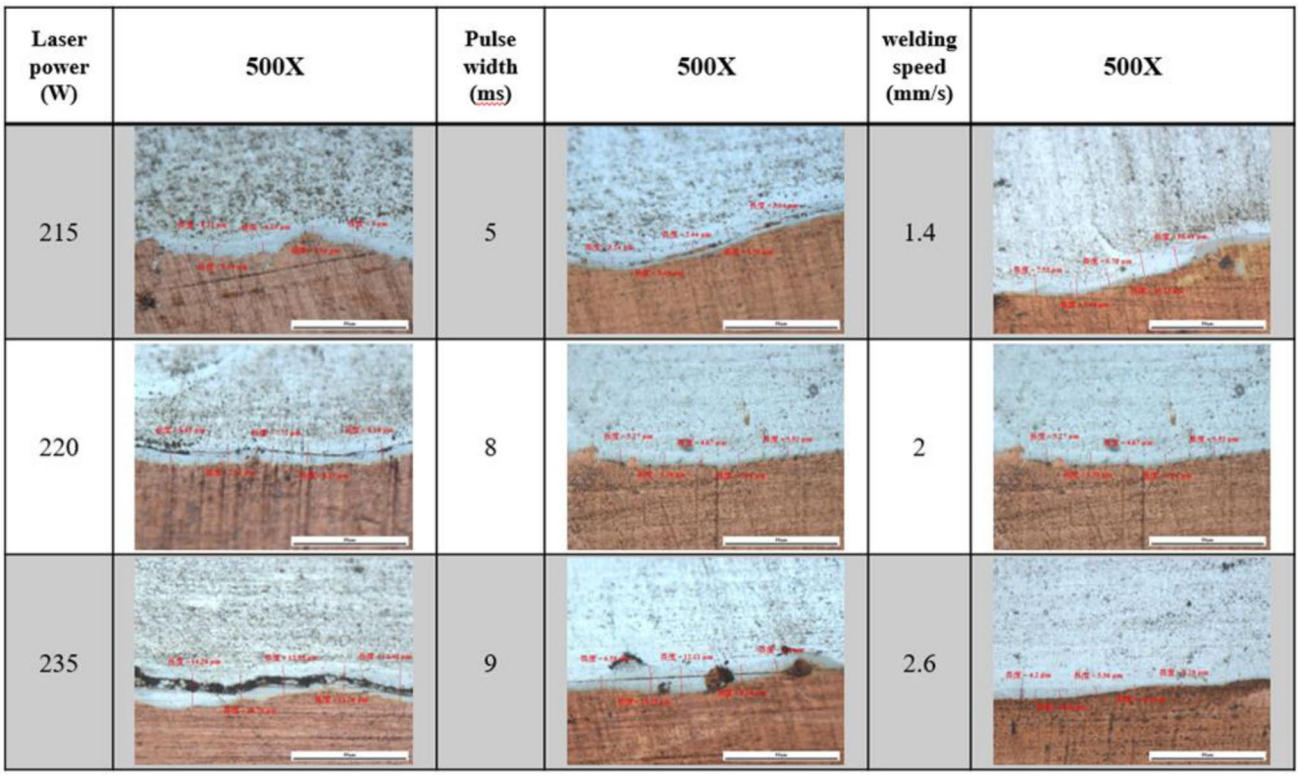

Fig. 13 OM images of IMC layers in welded samples produced using different LBW processing parameters

Figure 12b shows the micro-Vickers hardness profiles along the three depth planes indicated in Fig. 12a. A significant increase in the hardness is observed in the interface region of the weld. Hence, it is inferred that the welding process prompts the formation of an IMC layer in the weld bead. It is noted that this inference is consistent with the findings of Shi et al. [14] that the occurrence of Marangoni convection during the fabrication of dissimilar Cu–Al welds leads to the formation of a Cu–Al eutectic zone with increased hardness.

Previous studies have shown that the thickness of the IMC layer is correlated with the mechanical and thermal properties of the welded joint [37, 38]. Figure 13 presents OM images of the IMC layers in samples produced using various values of the laser power, pulse width, and welding speed. Figure 14a–c shows the correlations between the tensile strength and the IMC thickness for samples produced with different laser powers, pulse widths, and welding speeds, respectively. (Note that for each parameter setting, three samples were produced in order to ensure the reliability of the experimental results.) In general, the OM images in Fig. 13 show that the propensity of the weld bead to cracking at the Cu–Al interface is enhanced at either a low IMC layer thickness or a high IMC layer thickness. Meanwhile, the results presented in Fig. 14 reveal that the optimal processing conditions result in an IMC layer thickness close to 6 μm and produce the maximum tensile strength among all the considered samples. Figures 15 and 16 show the SEM–EDS and XRD analysis results for the interfacial region of the optimal dissimilar Cu–Al joint. The EDS and XRD results confirm that, in addition to pure Cu and Al, the interfacial region contains Al_2Cu IMC phase.

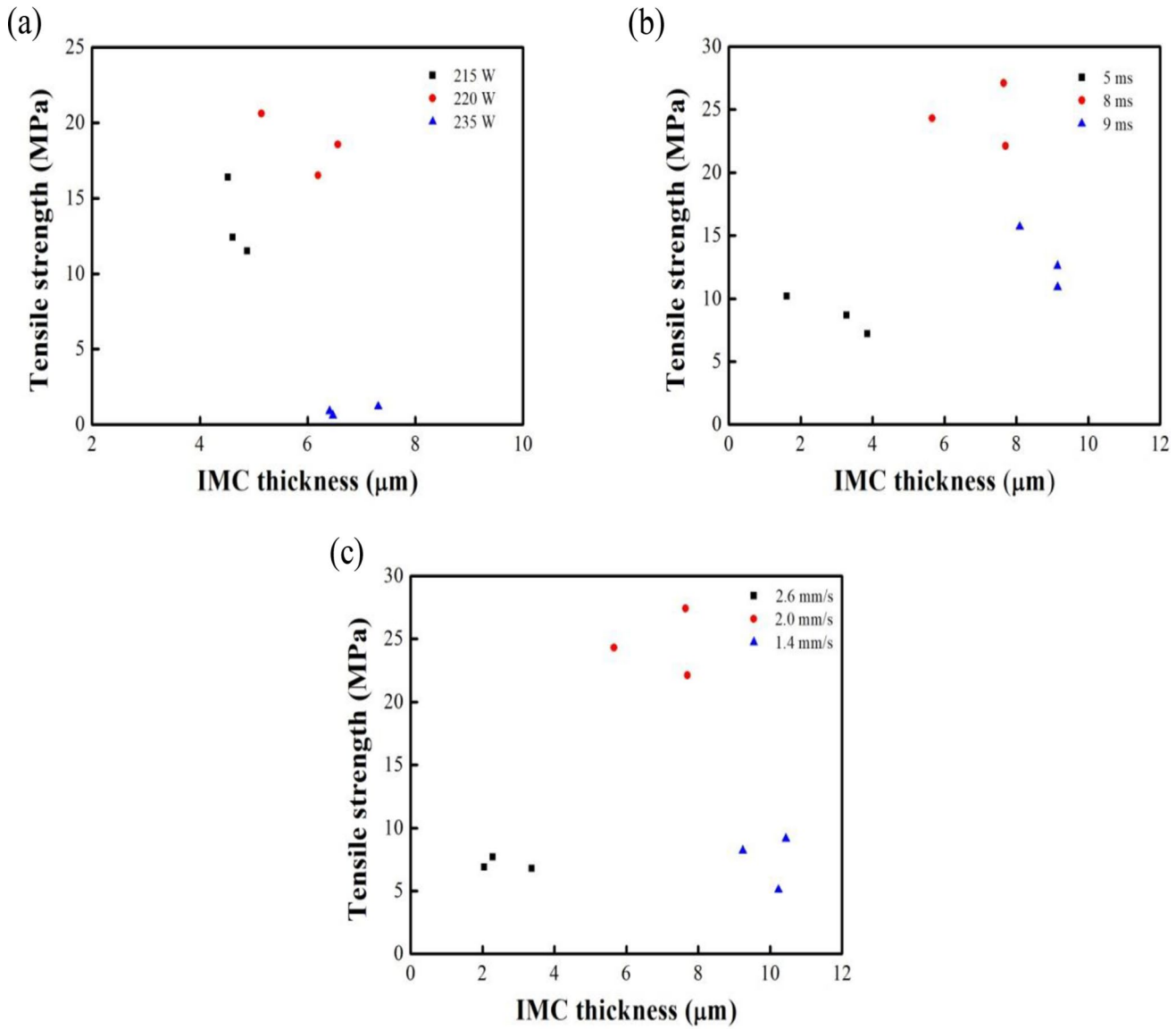

Fig. 14 Correlation between tensile strength and IMC layer thickness for different: (**a**) laser powers, (**b**) pulse widths, and (**c**) welding speeds

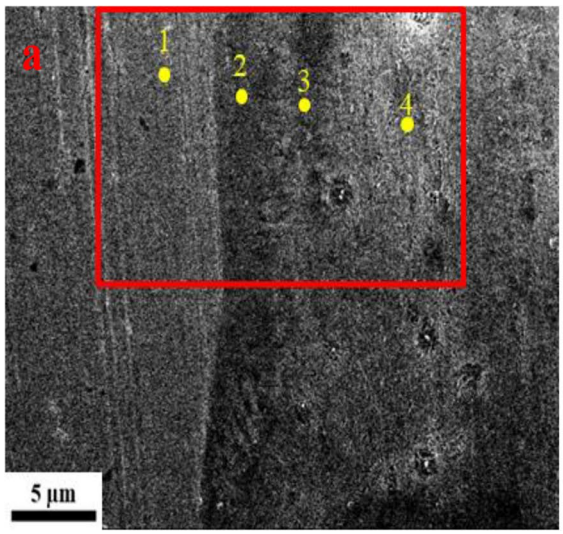

b

Marker	Wt% Al	Wt% Cu	Possible phase
EDS1	1.06	97.81	Cu
EDS2	42.29	56.30	$\theta(Al_2Cu)$
EDS3	55.55	41.82	$Al+\theta(Al_2Cu)$
EDS4	77.45	20.73	$Al+\theta(Al_2Cu)$

Fig. 15 (**a**) SEM image and (**b**) corresponding EDS analysis results for weld bead produced using optimal LBW processing parameters

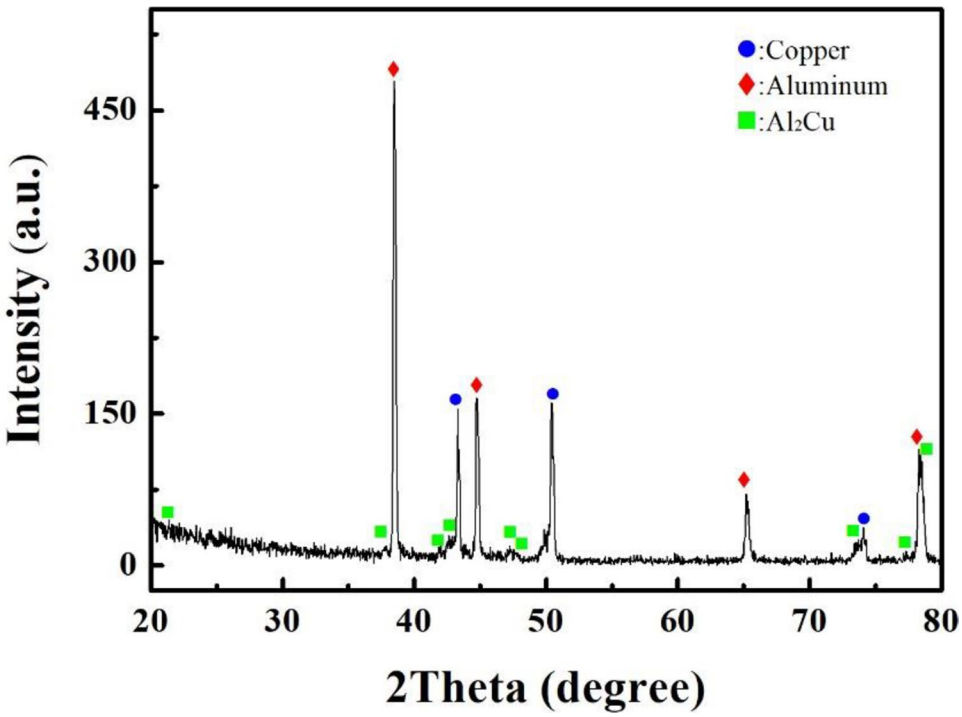

Fig. 16 X-ray diffraction pattern for weld bead produced using optimal LBW processing parameters

4 Conclusions

This study has conducted an experimental investigation into the effects of the LBW processing parameters on the mechanical and thermal properties of copper–aluminum composite heat sink assemblies. The experimental results support the following major conclusions:

(1) The optimal processing conditions are a laser power of 220 W, a pulse width of 8 ms, a welding speed of 2 mm/s, and an incident angle of 60°.
(2) The optimal processing conditions increase the weld penetration at the copper–aluminum interface and minimize the formation of cracks and voids in the weld bead. As a result, both the tensile strength and

the thermal conductivity of the heat sink assembly are effectively improved. The tensile strength and heating rate of the weld produced using the optimal welding parameters are 24.31 MPa and 41.2 °C/10^2 S, respectively.

(3) The experimental thermal conductivity of the heat sink fabricated under the optimal processing conditions is close to that of the ideal heat sink assembly.

(4) The optimal processing conditions result in the formation of an IMC layer with a thickness of approximately 6 μm. The EDS and XRD analysis results show that the IMC layer consists mainly of Al_2Cu eutectic phase.

Author contribution CLC: resources, review, and visualization. YHC: investigation, formal analysis, data collection, visualization, and writing. HKL: writing, review, and funding acquisition.

Funding The authors received financial support provided by the Ministry of Science and Technology of Taiwan, ROC, under Project No. MOST 110–2221-E-020–011.

Data availability All data generated or analyzed during this study are included in the present article.

Declarations

Ethics approval Not applicable.

Consent to participate Not applicable.

Consent for publication Not applicable.

Competing interests The authors declare no competing interests.

References

1. Shi Y, Wu S, Liao H, Wang X (2020) Microstructure and mechanical properties of CLF-1/316 L steel dissimilar joints welded with fiber laser welding. J Manuf Process 54:318–327
2. Cao X, Wallace W, Poon C, Immarigeon JP (2003) Research and progress in laser welding of wrought aluminum alloys. I. Laser Welding Processes. Mater Manuf Process 18(1):1–22
3. Mazumder WMSJ (2010) Laser material processing. Springer, London Dordrecht Heidelberg New York
4. H.H.T. Graf, Laser In der Fertigung, Vieweg+Teubner | GWV Fachverlage GmbH, Wiesbaden 2009
5. Tariq A, Altaf K, Ahmad SW, Hussain G, Ratlamwala TAH (2021) Comparative numerical and experimental analysis of thermal and hydraulic performance of improved plate fin heat sinks. Appl Therm Eng 182:115949
6. Abbas A, Wang CC (2020) Augmentation of natural convection heat sink via using displacement design. Int J Heat Mass Transf 154:119757
7. Ansari D, Jeong JH (2020) A novel composite pinfin heat sink for hotspot mitigation. Int J Heat Mass Transf 156:119843
8. Di C, Huang S, Yu X, Xu L, Jiao K (2021) Effect of cutting tool materials on temperature field of cutting AF1410 high strength steel. J Ordnance Equip Eng 6:243–250
9. Zhou X, Zhang G, Shi Y, Zhu M, Yang F (2017) Microstructures and mechanical behavior of aluminum-copper lap joints. Mater Sci Eng, A 705:105–113
10. Zhang J, Huang T, Mironov S, Wang D, Zhang Q, Wu Q, Xu J, Xiao R (2021) Laser pressure welding of copper. Opt Laser Technol 134:106645
11. Weigl M, Schmidt M (2010) Influence of the feed rate and the lateral beam displacement on the joining quality of laser-welded copper-stainless steel connections. Phys Procedia 5:53–59
12. Solchenbach T, Plapper P (2013) Mechanical characteristics of laser braze-welded aluminium–copper connections. Opt Laser Technol 54:249–256
13. Kah P, Vimalraj C, Martikainen J, Suoranta R (2015) Factors influencing Al-Cu weld properties by intermetallic compound formation. Int J Mech Mater Eng 10:10
14. Yan S, Shi Y (2019) Influence of laser power on microstructure and mechanical property of laser-welded Al/Cu dissimilar lap joints. J Manuf Process 45:312–321
15. Xia H, Tan C, Tian R, Meng S, Li L, Ma N (2020) Influence of shielding gas on microstructure and mechanical properties of laser welded–brazed Al/steel lapped joint. J Manuf Process 54:347–358
16. Choudhury T, Ghorai A, Medhi T, Acharya U, Roy BS, Saha SC (2021) Study of microstructure and mechanical properties in friction stir welded aluminum copper lap joint. Materials Today: Proceedings 46:9474–9479
17. Yan S, Li Z, Song L, Zhang Y, Wei S (2023) Research and development status of laser micro-welding of aluminum-copper dissimilar metals: a review. Opt Lasers Eng 161:107312
18. Hansen KS, Kristiansen M, Olsen FO (2014) Beam shaping to control of weldpool size in width and depth. Phys Procedia 56:467–476
19. Rasch M, Roider C, Kohl S, Strauß J, Maurer N, Nagulin KY, Schmidt M (2019) Shaped laser beam profiles for heat conduction welding of aluminium-copper alloys. Opt Lasers Eng 115:179–189
20. Geng Y, Akbari M, Karimipour A, Karimi A, Soleimani A, Afrand M (2019) Effects of the laser parameters on the mechanical properties and microstructure of weld joint in dissimilar pulsed laser welding of AISI 304 and AISI 420. Infrared Phys Technol 103:103081
21. Li Z, Rostam K, Panjehpour A, Akbari M, Karimipour A, Rostami S (2020) Experimental and numerical study of temperature field and molten pool dimensions in dissimilar thickness laser welding of Ti6Al4V alloy. J Manuf Process 49:438–446
22. Hu B, Richardson IM (2006) Mechanism and possible solution for transverse solidification cracking in laser welding of high strength aluminium alloys. Mater Sci Eng, A 429(1–2):287–294
23. Jia Z, Zhang P, Yu Z, Shi H, Liu H, Wu D, Ye X, Wang F, Tian Y (2021) Effect of pulse shaping on solidification process and crack in 5083 aluminum alloy by pulsed laser welding. Opt Laser Technol 134:106608
24. Yang ZB, Tao W, Li LQ, Chen YB, Li FZ, Zhang YL (2012) Double-sided laser beam welded T-joints for aluminum aircraft fuselage panels: process, microstructure, and mechanical properties. Mater Des 33:652–658
25. Dimatteo V, Ascari A, Liverani E, Fortunato A (2022) Experimental investigation on the effect of spot diameter on continuous-wave laser welding of copper and aluminum thin sheets for battery manufacturing. Opt Laser Technol 145:107495
26. Sun T, Franciosa P, Ceglarek D (2021) Effect of focal position offset on joint integrity of AA1050 battery busbar assembly during remote laser welding. J Market Res 14:2715–2726

27. Ahn J, Chen L, He E, Dear JP, Davies CM (2018) Optimisation of process parameters and weld shape of high power Yb-fibre laser welded 2024–T3 aluminium alloy. J Manuf Process 34:70–85
28. Quintino L, Costa A, Miranda R, Yapp D, Kumar V, Kong CJ (2007) Welding with high power fiber lasers – A preliminary study. Mater Des 28(4):1231–1237
29. Katayama S (2018) Understanding and improving process control in pulsed and continuous wave laser welding. Adv Laser Mater Process pp 153–183
30. Lerra F, Ascari A, Fortunato A (2019) The influence of laser pulse shape and separation distance on dissimilar welding of Al and Cu films. J Manuf Process 45:331–339
31. Pellone L, Inamke G, Hong K-M, Shin YC (2019) Effects of interface gap and shielding gas on the quality of alloy AA6061 fiber laser lap weldings. J Mater Process Technol 268:201–212
32. Beiranvand ZM, Ghaini FM, Naffakh-moosavy H, Sheikhi M, Torkamany MJ (2018) Magnesium loss in Nd:YAG pulsed laser welding of aluminum alloys. Metall and Mater Trans B 49(5):2896–2905
33. Çam G, İpekoğlu G (2016) Recent developments in joining of aluminum alloys. Int J Adv Manuf Technol 91(5–8):1851–1866
34. Bergmann JP, Bielenin M, Stambke M, Feustel T, Witzendorff PV, Hermsdorf J (2013) Effects of diode laser superposition on pulsed laser welding of aluminum. Physics Procedia 41:180–189
35. Dimatteo V, Ascari A, Fortunato A (2019) Continuous laser welding with spatial beam oscillation of dissimilar thin sheet materials (Al-Cu and Cu-Al): process optimization and characterization. J Manuf Process 44:158–165
36. Meco S, Ganguly S, Williams S, McPherson N (2019) Design of laser welding applied to T joints between steel and aluminium. J Mater Process Technol 268:132–139
37. Hou W, Shen Z, Huda N, Oheil M, Shen Y, Jahed H, Gerlich AP (2021) Enhancing metallurgical and mechanical properties of friction stir butt welded joints of Al–Cu via cold sprayed Ni interlayer. Mater Sci Eng: A 809:140992
38. Jimenez-Mena N, Jacques PJ, Ding L, Gauquelin N, Schryvers D, Idrissi H, Delannay F, Simar A (2019) Enhancement of toughness of Al-to-steel friction melt bonded welds via metallic interlayers. Mater Sci Eng, A 740–741:274–284